

A novel autophagy modulator 6-Bio ameliorates SNCA/ α -synuclein toxicity

S. N. Suresh^a, Aravinda K. Chavalmane^{a,†}, Vidyadhara DJ^c, Haorei Yarreiphang^c, Shashank Rai^{a,††}, Abhik Paul^b, James P. Clement^b, Phalguni Anand Alladi^c, and Ravi Manjithaya^{a,b}

^aMolecular Biology and Genetics Unit, Jawaharlal Nehru Centre for Advanced Scientific Research, Jakkur, Bangalore, India; ^bNeuroscience Unit, Jawaharlal Nehru Centre for Advanced Scientific Research, Jakkur, Bangalore, India; ^cDepartment of Neurophysiology, National Institute of Mental Health and Neuro Sciences, Bangalore, India

ABSTRACT

Parkinson disease (PD) is a life-threatening neurodegenerative movement disorder with unmet therapeutic intervention. We have identified a small molecule autophagy modulator, 6-Bio that shows clearance of toxic SNCA/ α -synuclein (a protein implicated in synucleopathies) aggregates in yeast and mammalian cell lines. 6-Bio induces autophagy and dramatically enhances autolysosome formation resulting in SNCA degradation. Importantly, neuroprotective function of 6-Bio as envisaged by immunohistology and behavior analyses in a preclinical model of PD where it induces autophagy in dopaminergic (DAergic) neurons of mice midbrain to clear toxic protein aggregates suggesting that it could be a potential therapeutic candidate for protein conformational disorders.

ARTICLE HISTORY

Received 14 March 2016
Revised 30 January 2017
Accepted 28 February 2017

KEYWORDS

6-Bio; autolysosomes; autophagy; high-throughput screening; MPTP; neurodegeneration, SNCA; TH



Introduction


Parkinson disease is the second most common neurodegenerative disorder affecting 1% of the aging population.¹ Motor abnormalities which are the major clinical clues for PD are first manifested when about 60% of the nigral DAergic neurons are lost,² decreasing dopamine levels. Although L-DOPA has been recommended for PD patients, it does not halt neurodegeneration. Furthermore, the predominant side effect of continuous L-DOPA administration is an occurrence of L-DOPA-induced dyskinesia among PD patients.³ Thus, there is an absolute need for better therapeutic agents to be made available for PD patients, aiming to stop or reduce neurodegeneration.

One of the hallmarks of PD is formation of misfolded protein aggregates (Lewy bodies) due to overexpressed SNCA or mutation in genes such as *PINK1* (PTEN induced putative kinase 1), *LRRK2* (leucine rich repeat kinase 2) that leads to death of DAergic neurons. The accumulation of these aggregates disrupts proteostasis machineries such as chaperones, proteasome or macroautophagy (hereafter autophagy) leading to neuronal degeneration.⁴ Misfolded SNCA aggregates are refractory to proteostasis maintaining processes and the resultant cytotoxicity is further exasperated by aging, as unlike mitotic cells, nondividing neurons cannot dilute out these aggregates.⁴ In accordance, neuronal specific loss of autophagy function leads to aggregate formation and subsequent neurodegeneration suggesting a role for basal autophagy in preventing aggregate

buildup.^{5–7} As autophagy is dysfunctional in many neurodegenerative disorders,⁴ several studies have pointed out that restoring proteostasis by upregulating autophagy can eliminate these protein aggregates and restore cellular homeostasis.^{8–10}

One of the main causes of this disease is the toxic buildup of protein aggregates leading to neuronal death. We screened for small molecule drug-like compounds that clear such protein aggregates (aggrephagy) and restore cell viability. Several model systems were used to identify and evaluate the small molecules for aggrephagy. Toward this, rather than a conventional structure based drug designing, we sought for a phenotypic-based small molecule screening in yeast and validated the results in higher model systems. In this study, we identified a small molecule 6-Bio for its ability to clear SNCA aggregates and restore cellular homeostasis. We further show that 6-Bio induces autophagy and strongly drives autophagy flux resulting in aggregate clearance. We elucidated that 6-Bio modulates autophagy flux through inhibiting GSK3B activity. GSK3B has been associated with Alzheimer disease pathogenesis by modulating 2 processes namely (i) β -amyloid buildup and (ii) formation of neurofibrillary tangles.¹¹ It has been demonstrated at cellular level experiments that inhibiting GSK3B would ablate the expression of SNCA¹² suggesting its role in synucleopathies. Finally, in a pre-clinical mouse model of PD, 6-Bio showed potent neuroprotective ability revealed by immunohistological and behavior analyses.

CONTACT Ravi Manjithaya  ravim@jncsar.ac.in  Assistant Professor (Faculty Fellow), Molecular Biology and Genetics Unit, Associate Faculty, Neuroscience Unit, Jawaharlal Nehru Centre for Advanced Scientific Research, Jakkur, Bangalore 560 064, India.

 Supplemental data for this article can be accessed on the [publisher's website](#).

[†]Present address - School of Biological Sciences, Nanyang Technological University, Singapore.

^{††}Present address - Bio-Medical Research Centre, Faculty of Medicine and Health, University of East Anglia, United Kingdom.

© Jawaharlal Nehru Centre for Advanced Scientific Research. Published with license by Taylor & Francis.

This is an Open Access article distributed under the terms of the Creative Commons Attribution-Non-Commercial License (<http://creativecommons.org/licenses/by-nc/3.0/>), which permits unrestricted non-commercial use, distribution, and reproduction in any medium, provided the original work is properly cited. The moral rights of the named author(s) have been asserted.

Results

Small-molecule screening reveals 6-Bio as a potent inducer of autophagy

The occurrence of protein aggregates and cytotoxicity by SNCA overexpression is also recapitulated in the budding yeast, *Saccharomyces cerevisiae* (Fig. S1, A to C).¹³ We used this “out-of-the-box” yeast model¹⁴ to screen for small molecules that would prevent cytotoxicity by aggregate degradation. We screened a small molecule library containing pharmacologically active compounds (LOPAC¹²⁸⁰) using an SNCA yeast toxicity assay (Fig. 1A, Fig. S2). Of the hits that rescued growth in this model was the SIRT2 inhibitor AGK2, which was shown to rescue SNCA toxicity¹⁵ affirming the reliability of the assay, and the compound 6-Bio [(2′Z,3′E)-6-Bromoindirubin-3′-oxime]¹⁶ (Fig. S3A). Interestingly, 6-Bio did not affect the growth of yeast cells (Fig. 1B). To understand the involvement of 6-Bio in autophagy, GFP-Atg8 (GFP tagged autophagy-related 8, a yeast autophagosome marker)-processing assay under both growth and starvation conditions were used. During growth conditions where autophagy is barely detectable, 6-Bio dramatically induced autophagy (6 h time point, $P < 0.001$ vs untreated; Fig. 1C) and also the flux (6 h time point, $P < 0.001$ vs untreated; Fig. 1C). Similarly, 6-Bio treatment under starvation condition showed significant increase in autophagy induction (4 h and 6 h time points, $P < 0.001$ vs untreated; Fig. 1D) and flux (4 h and 6 h time points, $P < 0.01$ and $P < 0.001$, respectively vs untreated; Fig. 1D) by 2-fold in a time-dependent manner suggesting 6-Bio augmented starvation-induced autophagy.

We further tested 6-Bio for autophagy modulation in mammalian cells. Toward this, we used MAP1LC3B/LC3B (microtubule associated protein 1 light chain 3 β , a mammalian autophagosome marker and an ortholog of yeast Atg8) processing and tandem RFP-GFP-LC3B assays. In HeLa cells, 6-Bio increased LC3B-II (the autophagosome-associated, processed form of LC3B-I) levels in a dose-dependent manner suggesting autophagy modulation (Fig. 3A). In the presence of lysosomal protease inhibitors, E64D and pepstatin A, LC3B-II accumulation was significantly more than that of 6-Bio only and/or E64D and pepstatin A only (Fig. S9, A and B), validating that 6-Bio is indeed an autophagy enhancer. In the tandem RFP-GFP-LC3B assay that reveals autophagy flux, 6-Bio treatment dramatically increased autolysosome numbers (~9-fold, $P < 0.001$, compared with control; Fig. 1E) indicating enhanced fusion of autophagosomes with lysosomes.

Next, we checked whether the lysosomal functions are perturbed by 6-Bio since it specifically enhances autolysosomes. For this, we checked the lysosomal pH by LysoTracker Deep Red staining upon 6-Bio treatment. HeLa cells were treated with 6-Bio and/or E64D plus pepstatin A for 2 h, followed by treatment with LysoTracker Deep Red for 20 min. LysoTracker Deep Red fluorescence intensity was reduced in presence of protease inhibitors such as E64D and pepstatin A (Pep A). The fluorescence intensity of LysoTracker Deep Red was found to be comparable between untreated and 6-Bio-treated cells (Fig. S10B). Thus, we found no difference in both E64D + pep A only, 6-Bio and E64D + pep A treatments (Fig. S10B).

LysoTracker Deep Red staining indicated that there was no change in lysosome acidification (Fig. S10). LAMP1 (lysosomal associated membrane protein 1)-positive vesicle intensities and distribution also were unaltered upon 6-Bio treatment suggesting that perhaps lysosomal functions were not perturbed by 6-Bio (Fig. S10A).

To address whether the molecule enters the cell via endocytosis, we performed the tandem RFP-GFP-LC3B assay at 16°C. At this temperature, endocytosis pathway is highly reduced as evident by the significantly decreased cellular uptake of FITC-dextran (70 kDa) as compared with 37°C (Fig. S11C). However, the effect of 6-Bio in increasing fusion between autophagosomes and lysosomes at 37°C (~10-fold, control vs 6-Bio-treated, $P < 0.001$, Fig. S11, A and B) and 16°C (~8-fold, control vs 6-Bio-treated, $P < 0.001$, Fig. S11, A and B) were comparable suggesting that endocytosis did not play a predominant role in the action of 6-Bio in modulating autophagy. These results suggest that 6-Bio affects autophagy independent of endocytosis perhaps by passive diffusion.

From these 2 model systems, we noticed that 6-Bio not only induces autophagy but also enhances starvation-induced autophagy and strikingly promotes autolysosome formation without perturbing the lysosomal function.

6-Bio clears SNCA in an autophagy-dependent manner

Treatment of yeast cells overexpressing SNCA-GFP with 6-Bio, resulted in vacuolar degradation of SNCA-GFP cytosolic aggregates with improved normal plasma membrane localization suggesting possible involvement of autophagy-related pathways (Fig. 2A). In agreement with these observations, 6-Bio failed to rescue the SNCA-mediated toxicity in autophagy gene mutants (*atg1Δ*, *atg5Δ*, *atg8Δ*, *atg11Δ* and *atg15Δ*) (Fig. S3B).

Assays performed to monitor degradation of SNCA-GFP aggregates in presence of 6-Bio under nonstarvation and starvation conditions revealed a time-dependent and significant decrease in the SNCA-GFP levels in wild-type cells (Fig. 2, B and D and Fig. S4, B and C) but not in an autophagy mutant, *atg1Δ* (Fig. 2, C and E and Fig. S4, D and E). These results suggest that 6-Bio treatment was not only able to enhance starvation-induced autophagy but also resulted in a concomitant decrease of SNCA-GFP demonstrating that the prosurvival effects of 6-Bio was due to autophagy-dependent SNCA-GFP clearance.

Next, using an SNCA degradation assay model in a human neuroblastoma cell line (SH-SY5Y) overexpressing GFP-SNCA, we observed that 6-Bio significantly reduced GFP-SNCA levels (~2-fold, $P < 0.001$ vs untreated). However, in the presence of the autophagy inhibitor 3-methyladenine (3-MA), the GFP-SNCA levels did not change upon 6-Bio cotreatment suggesting that autophagy was the primary mechanism for degradation (as also seen in the yeast model) (Fig. 2, C and E; Fig. 2F and Fig. S4, D and E). As MTOR (mechanistic target of rapamycin) negatively controls autophagy, we tested if 6-Bio affected MTOR signaling. 6-Bio decreased phosphorylation levels of RPS6KB1/p70s6K (ribosomal protein S6 kinase B1) and EIF4EBP1/4E-BP1 (eukaryotic translation initiation factor 4E binding protein 1) in a dose-dependent manner (Fig. 3A),

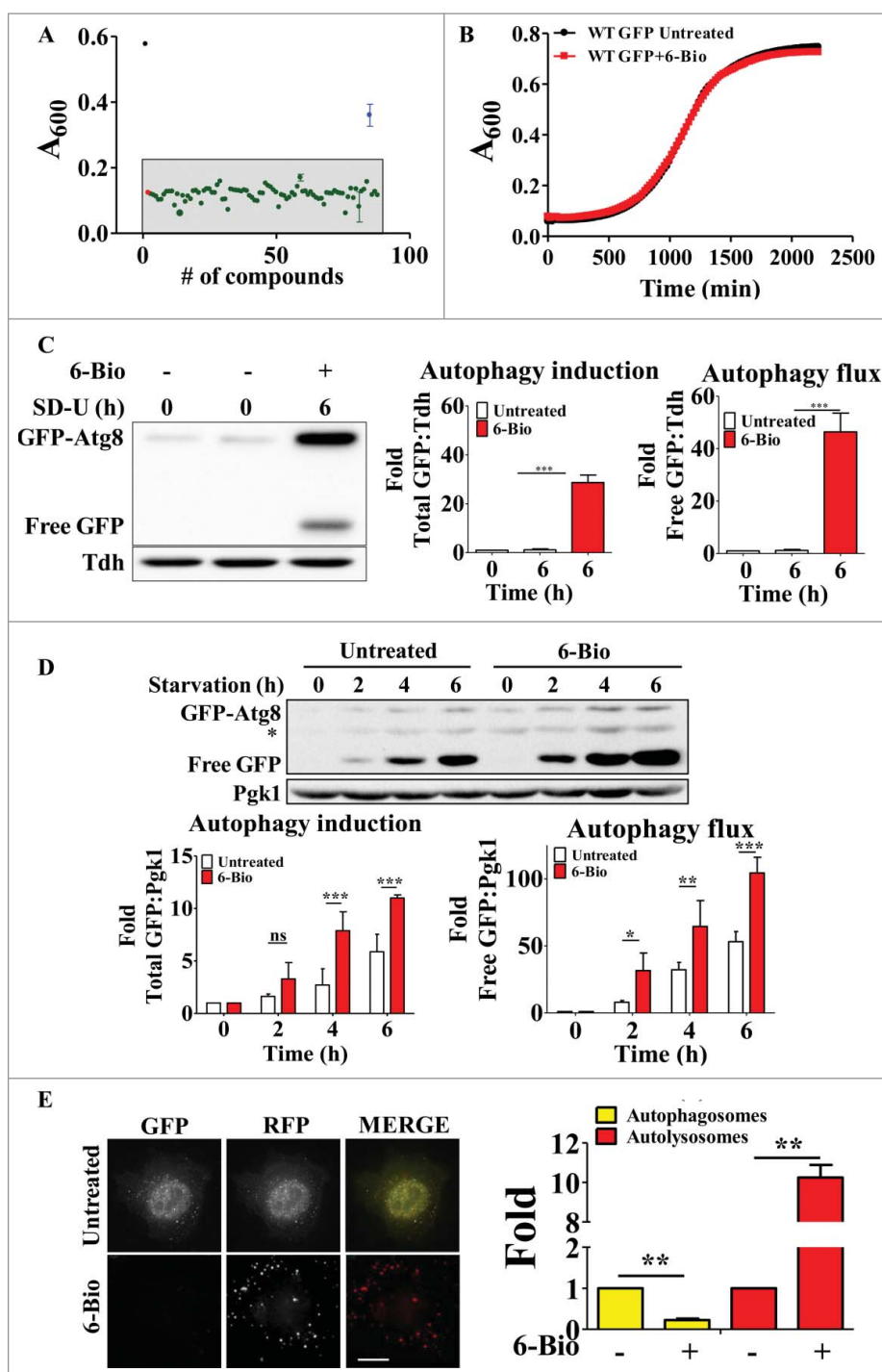


Figure 1. 6-Bio induces autophagy. (A) Box plot demonstrating hits from a small molecule library of pharmacologically active compounds, LOPAC¹²⁸⁰, screened in *S. cerevisiae* toxicity model of SNCA. Detailed screening methodology is explained in the methods section. In the box plot, compounds that rescued the growth (denoted by absorbance, A_{600}) of WT SNCA-GFP strains ≥ 3 SD units (gray box) are considered hits (blue) and the ones that do not are in green. WT GFP (black) and untreated WT SNCA-GFP (red) represent the positive and negative controls. A representative plot for 100 compounds is shown. (B) Growth curve of WT GFP cells with or without 6-Bio ($50 \mu\text{M}$) treatment. (C) Representative western blot of the GFP-Atg8-processing assay under growth condition. WT strain expressing GFP-Atg8 treated with or without 6-Bio ($50 \mu\text{M}$). Fusion protein GFP-Atg8 accumulation and free GFP release was monitored across the time course (0 and 6 h). Tdh reactivity served as a loading control. Representative graph for quantification of autophagic induction and flux ($n = 4$). (D) Representative western blot for the GFP-Atg8-processing assay. Fusion protein GFP-Atg8 accumulation and free GFP release monitored across the time course (0, 2, 4 and 6 h) under starvation conditions in the WT strain expressing GFP-Atg8 treated with 6-Bio ($50 \mu\text{M}$). Representative graph for quantification of autophagic induction and flux ($n = 3$); * indicates nonspecific band. Pgk1 was assessed as loading control. (E) Representative microscopy images of ptf LC3B transfected HeLa cells treated with 6-Bio ($5 \mu\text{M}$) and quantification of autophagosome and autolysosome indicating fold change over its untreated counterpart ($n = 25$), scale bar: $15 \mu\text{m}$. Statistical analysis was performed using the Student unpaired *t* test, 2-way ANOVA and the post-hoc Bonferroni test. Error bars, mean \pm SEM ns-nonsignificant, * $P < 0.05$, ** $P < 0.01$, *** $P < 0.001$.

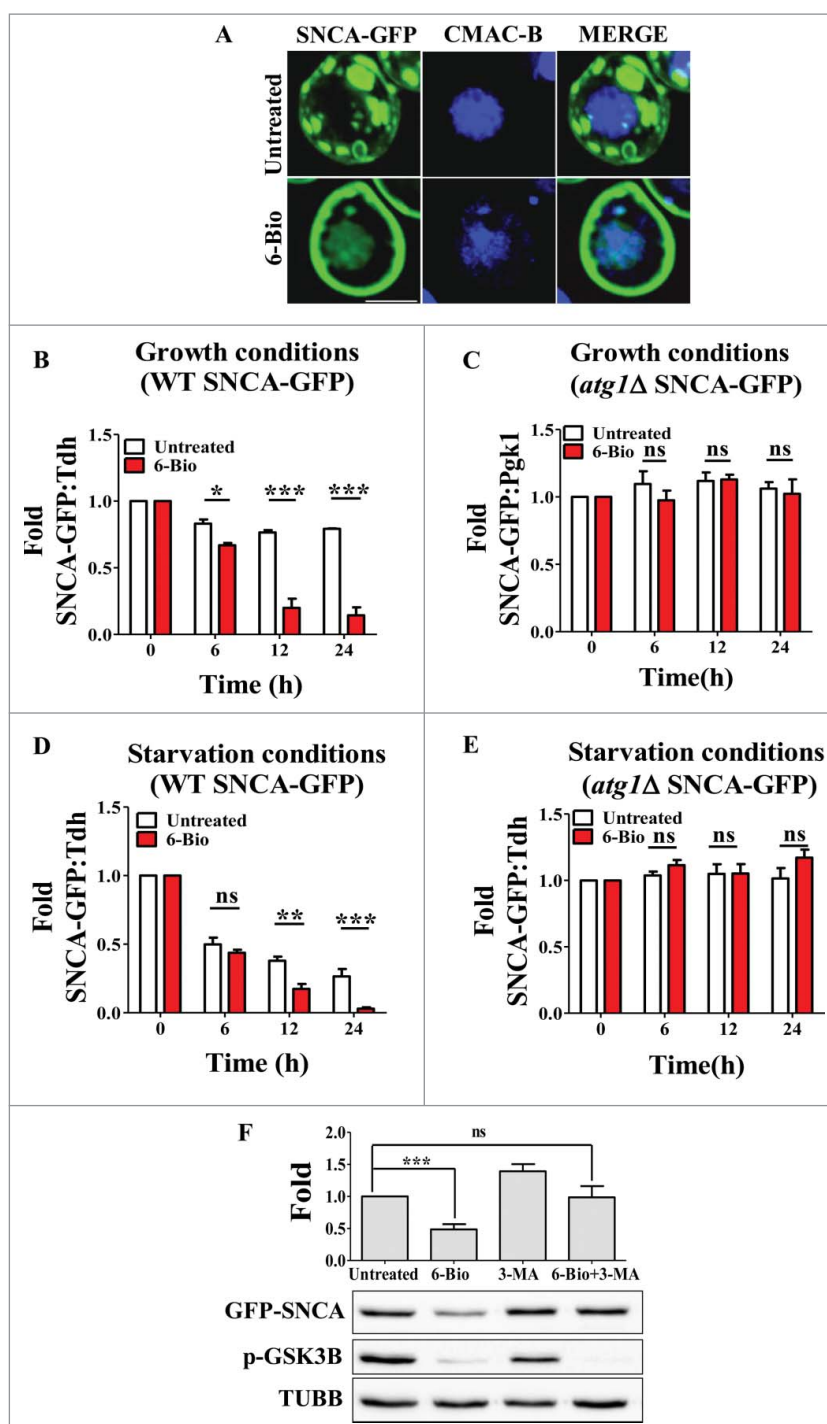


Figure 2. 6-Bio clears SNCA in an autophagy-dependent manner. (A) Microscopy images of WT SNCA-GFP yeast cells treated with or without 6-Bio (50 μ M) for 16 h, vacuole stained with CMAC-Blue (100 nM), scale bar: 2 μ m. (B) to (E) Quantification plots for SNCA-GFP degradation assay in wild-type (WT) yeast strain for growth (B) and starvation (D) conditions. SNCA-GFP degradation assay in the autophagy mutant (*atg1Δ*) strain under the given growth (C) and starvation (E) conditions (assay details are explained in Fig. S4A). SNCA-GFP protein levels after 6-Bio (50 μ M) treatment are analyzed for different time points (0, 6, 12 and 24 h). Tdh reactivity was used as loading control. (F) GFP-SNCA transiently transfected in SH-SY5Y cells were allowed to express for 24 h, treated with 6-Bio (5 μ M), 3-MA (5 mM) or both for 24 h post-transfection and assessed for GFP-SNCA degradation. Western blot (below) and graph (above) indicating fold change in GFP-SNCA degradation over untreated. TUBB was used as a loading control. Statistical analysis was performed using 2-way ANOVA and the post-hoc Bonferroni test. Error bars, mean \pm SEM ns-nonsignificant, * P < 0.05, ** P < 0.01, *** P < 0.001.

indicating 6-Bio negatively regulated MTOR signaling. During normal growth conditions, MTOR is active (and phosphorylates RPS6KB1 and EIF4EBP1) and autophagy is suppressed. Addition of 6-Bio results in autophagy induction by suppression of MTOR activity as revealed by diminished phosphorylation of its substrates RPS6KB1 and EIF4EBP1. 6-Bio is a potent

GSK3B inhibitor and reduced phosphorylated (p)-GSK3B indicates its reduced activity¹⁷ (Fig. 3A and Fig. 2F). These assays confirmed that 6-Bio treatment not only induced autophagy but also enhanced the autophagic flux by promoting autophagosome fusion with lysosomes in an MTOR-dependent manner.

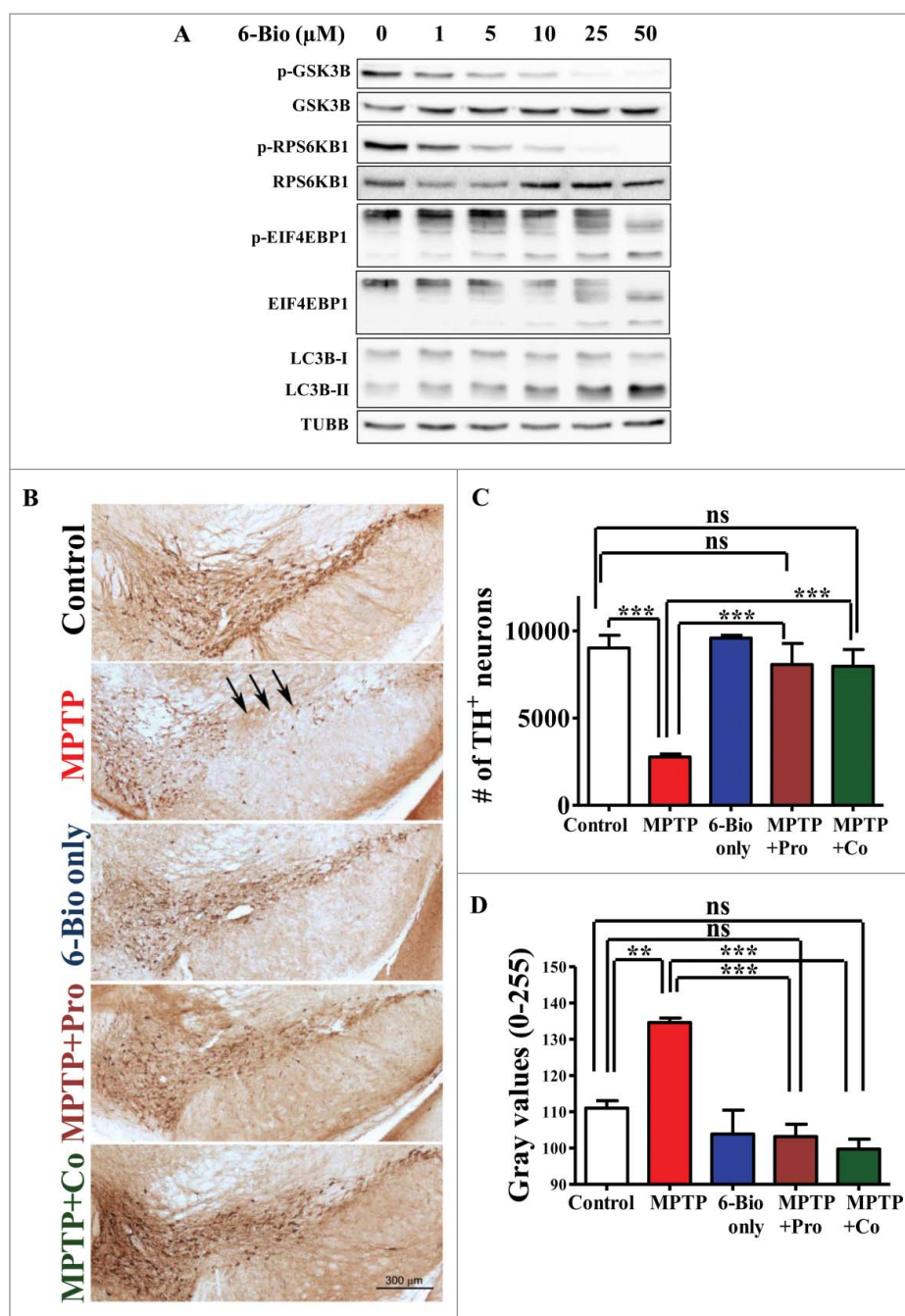


Figure 3. 6-Bio enhances MTOR-dependent autophagy and confers neuroprotection in a mouse MPTP toxicity model. (A) Representative western blots indicating dose-dependent modulation of autophagy related proteins (LC3B, RPS6KB1 and EIF4EBP1) by 6-Bio in HeLa cells. TUBB was used as a loading control. (B) to (D) Representative photomicrographs of TH⁺ immunostained DAergic neurons (B) in SNpc (arrow) of mouse midbrain. Placebo control cohort, MPTP-treated (23.4 mg/kg body weight), 6-Bio (5 mg/kg body weight) or both [Prophylaxis (MPTP+Pro)/Coadministration (MPTP+Co)], scale bar: 300 μm. Stereological (C) and densitometric quantification (D) indicating the number of TH⁺ DAergic neurons and their intensity in SNpc neurons. Statistical analysis was performed using the Student unpaired *t* test, one-way ANOVA and the post-hoc Bonferroni test. Scale bar: 50 μm. Error bars, mean ± SEM ns-nonsignificant, ***P* < 0.01, ****P* < 0.001.

Autophagy-dependent GSK3B-mediated neuro(cyto) protection by 6-Bio

We observed the significant reduction of GSK3B activity upon 6-Bio treatment as revealed by the reduced p-GSK3B levels (Fig. 2F and Fig. 3A). To understand the GSK3B dependency of autophagic activity by 6-Bio, we performed the knockdown studies in SH-SY5Y cells. For this, GSK3B shRNA was transiently transfected into cells and after 48 h the GSK3B protein levels were reduced significantly (Fig. S8A). In SH-SY5Y cells,

when SNCA was overexpressed for 72 h, the cell viability was significantly affected (Fig. S8D). When these cells were treated with 6-Bio, its viability was significantly increased and comparable to that of control (Fig. S7). Similar protection was noted in GSK3B-silenced SNCA-overexpressing cells. When GSK3B expression was silenced, addition of 6-Bio only showed marginal cytoprotection as compared with untreated cells with normal GSK3B expression (Fig. S8D). In fact, in silenced cells, 6-Bio was not effective in cytoprotection over and above that offered by silencing GSK3B but was cytotoxic (Fig. S8D). In

addition, another GSK3B inhibitor, compound VIII also exerted protection against SNCA-mediated toxicity (Fig. S8D). Using a direct readout for autophagy (tandem RFP-GFP-LC3B assay), we used a similar silencing strategy to address the GSK3B and autophagy interplay in the presence of 6-Bio. In GSK3B-silenced cells, the autolysosomes were increased with concomitant reduction in autophagosomes than that of its scrambled shRNA control ($P < 0.001$, Fig. S8, B and C). Interestingly, the autophagosomes and autolysosomes formed in GSK3B-silenced cells were similar to that of 6-Bio treatment. Notably, the autolysosomes formed in 6-Bio-treated, GSK3B-silenced cells were significantly reduced than that of cells treated only with 6-Bio ($P < 0.001$, Fig. S8, B and C). Although 6-Bio is known to affect other signaling pathways such as PDK1 (pyruvate dehydrogenase kinase 1) and JAK-STAT3 [(Janus kinase)-(signal transducer and activator of transcription 3)],¹⁸ our results suggest that 6-Bio primarily modulates autophagy in a GSK3B-dependent manner.

6-Bio confers neuroprotection in a mouse MPTP-toxicity model

We then investigated the effect of 6-Bio in one of the widely used preclinical models of PD, MPTP (1-methyl-4-phenyl-1,2,3,6-tetrahydropyridine) mouse model.¹⁹ It was reported that 7 d post MPTP administration results in ~70% DAergic neuronal loss in the substantia nigra pars compacta (SNpc) region of brain which leads to 80% to 90% reduction in dopamine levels in the striatum.¹⁹ In this model, 6-Bio was administered [5mg/kg, intraperitoneally (i.p.)] in 2 different regimen (Fig. S5A): on the same day of MPTP injections (coadministration, Co) or 2 d prior (prophylactic, Pro). In both cases, 6-Bio treatment was continued for 7 d post- MPTP administration. We then evaluated the status of DAergic neurons in SNpc. These neurons were identified by TH (tyrosine hydroxylase) immunolabeling and were quantitated by unbiased stereology and densitometry analysis. As expected, the number and health of DAergic neurons (as revealed by TH staining intensities) were significantly reduced in MPTP-treated mice (~3-fold, $P < 0.001$ compared with placebo; Fig. 3, B to D and Fig. S5B). Strikingly, in both the 6-Bio treatment regimen, the number of DAergic neurons resembled almost that of placebo or animals injected with 6-Bio only (Co or Pro ~2.5-fold vs MPTP, $P < 0.001$; Fig. 3, B to D and Fig. S5B). In addition, the decrease in SNpc volume upon MPTP administration was not seen in 6-Bio-treated cohort ($P < 0.001$ vs Co, $P < 0.01$ vs Pro; Fig. S5C). These observations in mouse model of PD reassert the neuroprotective nature of 6-Bio.

6-Bio enhances autophagy and clears toxic protein aggregates in mouse brains

We then evaluated the autophagy and toxic aggregate levels in the DAergic neurons in SNpc of midbrain. We observed the significant reduction of LC3B puncta per neuron in the MPTP-treated cohort than that of placebo (~1.8-fold, placebo vs MPTP, $P < 0.001$, Fig. 4, A and B). Conversely, APP/amyloid β oligomer/A11 puncta were significantly higher (~7-fold, placebo vs MPTP, $P < 0.001$, Fig. 4, C and D). Along with

decreased autophagy, these SNpc (TH⁺) neurons displayed toxic aggregate buildup. This reduced autophagy upon administration of MPTP is in agreement with previous observations.²⁰ Furthermore, as seen in cell culture models, 6-Bio treatment alone increased LC3B puncta per neuron (~2-fold, placebo vs 6-Bio only, $P < 0.001$, Fig. 4, A and B) suggesting that 6-Bio could induce autophagy in mice brain by crossing the blood-brain barrier (Fig. S13). When 6-Bio was coadministered along with MPTP, LC3B puncta per neuron increased (~2.5-fold, MPTP vs MPTP+Co, $P < 0.001$, Fig. 4, A and B) with a significant reduction in APP/amyloid β oligomer/A11-positive aggregates (~7-fold, MPTP vs MPTP+Co cohort, Fig. 4, C and D). Strikingly, the aggregate numbers in MPTP+Co were comparable to that of control suggesting that the 6-Bio treatment decreased the toxic aggregates to that of placebo neurons (placebo vs MPTP+Co, ns, $P > 0.05$, Fig. 4, C and D). These results imply that autophagy was drastically induced in the MPTP and 6-Bio coadministered cohort that lead to neuroprotection by clearance of the toxic aggregates. We observed reduced p-GSK3B signals in DAergic neurons of the 6-Bio-treated cohorts, namely, 6-Bio only and MPTP+Co (Fig. S13).

6-Bio ameliorates MPTP-induced behavioral deficits

To study whether 6-Bio can combat the MPTP-induced behavioral impairments in motor coordination, locomotion and exploration abilities, we used 2 widely used behavior tests namely rotarod and the open field test. Stereology were performed on d 7 post MPTP or placebo administrations, thus behavior experiments were conducted on d 13 i.e., d 7 post MPTP or placebo administrations. Behavior study scheme is illustrated in Fig. S6.

In rotarod test, the latency to fall for MPTP cohort reduced significantly to that of placebo cohort on d 13 postadministration (MPTP vs placebo, $P < 0.001$, Fig. 5A and Fig. S6, A and B) validating the MPTP-induced motor deficits in mice. Strikingly, the latency to fall was increased in the 6-Bio-treated cohort compared with that of MPTP-treated cohort (Co vs MPTP, $P < 0.001$, Fig. 5A and Fig. S6, B and C). The latency to fall for the 6-Bio-treated cohort was comparable with the placebo cohort (Co d 7 vs placebo, $P > 0.05$, Fig. 5A and Fig. S6, A and C).

Similar to the lack of motor coordination observed in rotarod, the total distance traveled by MPTP-treated cohort in the open field test arena on d 13 postinjection was reduced significantly compared with that of placebo (MPTP vs placebo, $P < 0.001$, Fig. 5B, C and Fig. S6, A and B) affirming the MPTP-induced locomotion and exploratory impairments. These impairments were reduced after 6-Bio administration as the distance traveled by mice increased dramatically (Co vs MPTP, $P < 0.001$, Fig. 5, B and C and Fig. S6, B and C) and matched control cohorts (Co vs placebo, $P > 0.05$, Fig. 5, B and C and Fig. S6, A and C). MPTP-induced impairments were not protected by 6-Bio when administered after 48 h of MPTP (Post vs MPTP, $P > 0.05$, Fig. 5, D and E and Fig. S6, B and D).

Since the 6-Bio-treated cohort spent more time on the rotarod (as the placebo cohort) and traveled more distance in open field unlike MPTP-treated, we therefore, can infer that 6-Bio rescued the MPTP-induced motor, locomotion and

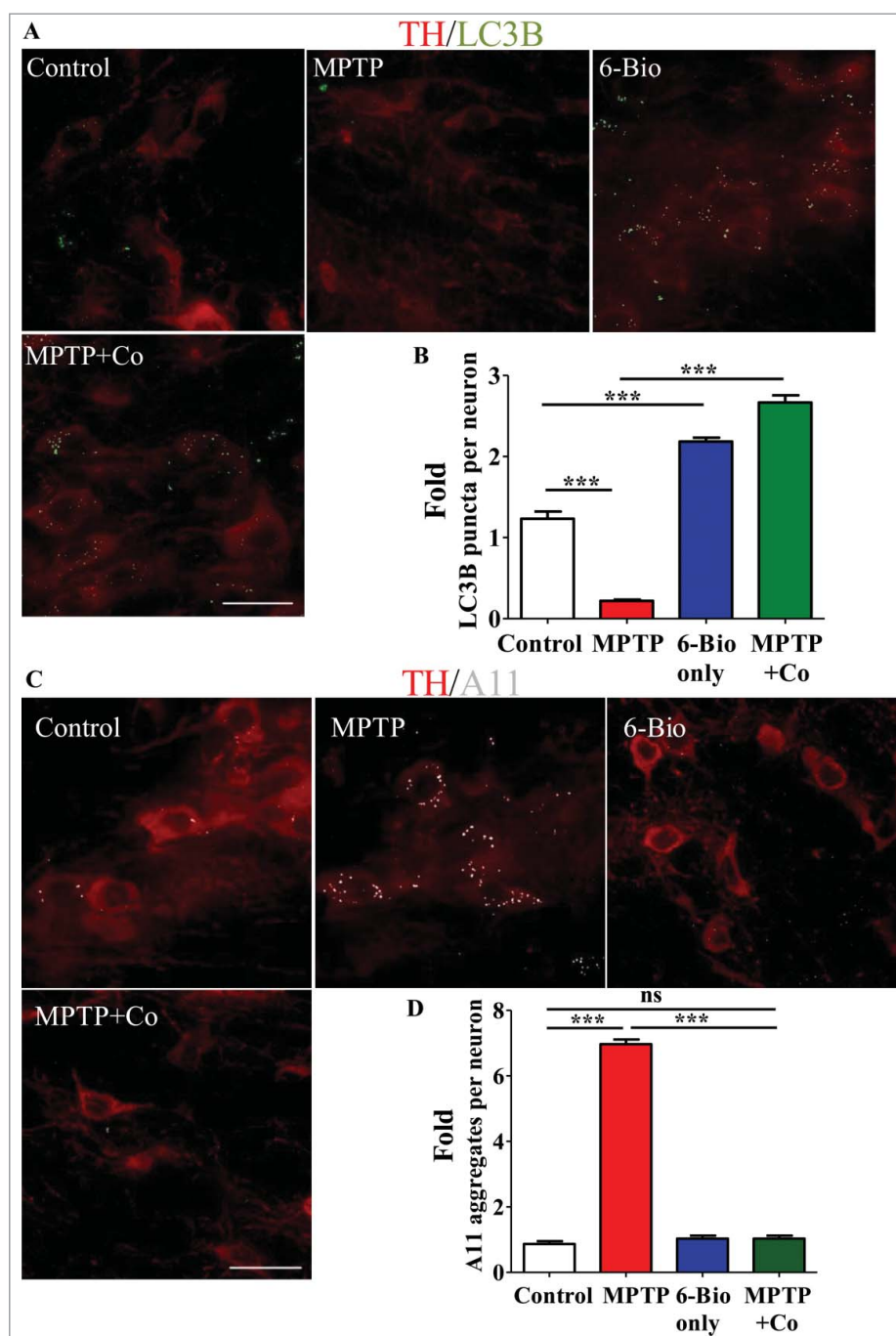


Figure 4. 6-Bio induces autophagy in mice brain to clear toxic protein aggregates. (A) Representative immunofluorescent photomicrographs of various cohorts namely control, MPTP (23.4 mg/kg of body weight), 6-Bio (5 mg/kg of body weight) and MPTP+Co that were stained for LC3B (an autophagy marker) and TH (SNpc) in midbrain. Autophagic modulation by 6-Bio were evaluated in DAergic neurons in SNpc and the LC3B puncta fold change per neuron was quantified (B). (C) Representative immunofluorescent photomicrographs of the above mentioned cohorts were stained for APP/amyloid β oligomer/A11 (toxic oligomers) and TH (SNpc) in midbrain. Aggregate clearance by 6-Bio were evaluated in DAergic neurons in SNpc and the APP/amyloid β oligomer/A11 puncta fold change per neuron was quantified (D). Statistical analysis was performed using one-way ANOVA and the post-hoc Bonferroni test. Scale bar: 50 μ m. Error bars, mean \pm SEM ns-nonsignificant, ***- $P < 0.001$.

exploratory impairments. We observed that 6-Bio failed to protect the MPTP-induced behavioral deficits when administered 48 h after MPTP dosage.

Discussion

Using an unbiased yeast high-throughput assay, we identified the small molecule 6-Bio that rescued SNCA cytotoxicity in an autophagy-dependent manner. 6-Bio induced autophagy even

in growth conditions. Mechanistically, 6-Bio profoundly promoted autophagosome-lysosome fusion as reflected in the high autolysosome numbers with hardly any unfused autophagosomes. Increased autophagy induction and fusion resulted in degradation and clearance of aggregated proteins with a concomitant rescue of cell viability and growth. When tested in a preclinical model of PD, 6-Bio demonstrated remarkable neuroprotection revealed by both immunohistology and behavioral analyses.

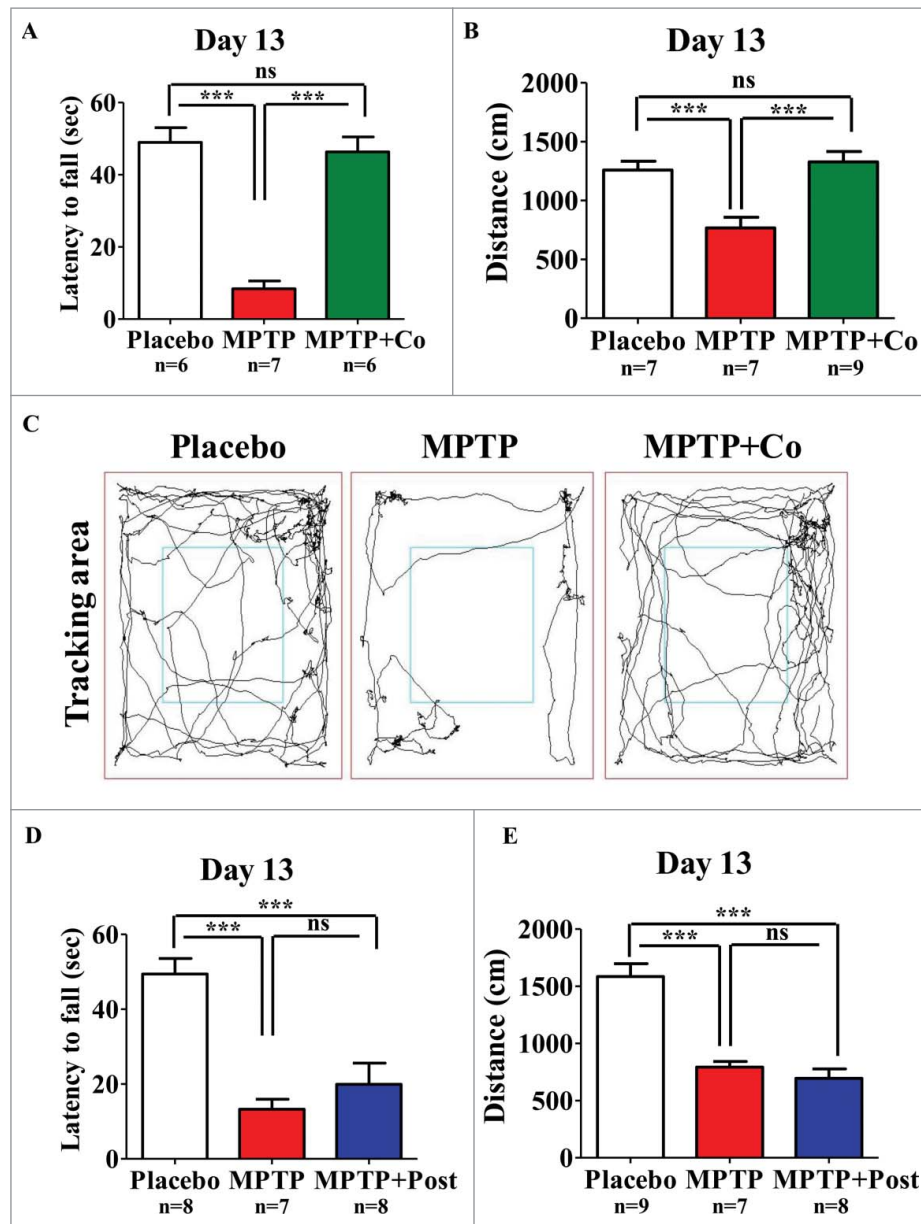


Figure 5. 6-Bio ameliorates MPTP-induced behavioral deficits. Effect of 6-Bio (5 mg/kg) on (A) latency to fall of various cohorts namely Placebo, MPTP and MPTP+Co as assessed by rotarod test (B) Representative trajectory maps of all mentioned cohorts as analyzed by open field test. (C) Periphery distance traveled by all indicated cohorts as assessed by open field test. Effect of 6-Bio (5 mg/kg) on various cohorts namely Placebo, MPTP and MPTP+Post. (D) latency to fall of various cohorts namely Placebo, MPTP and MPTP+Post as assessed by rotarod test. (E) Periphery distance traveled by all indicated cohorts as assessed by the open field test. Both the rotarod and open field behavior analyses were performed on d 13 or d 7 post MPTP or vehicle administrations. 6-Bio (5 mg/kg) was administered either along with MPTP (MPTP+Co) or post 48 h of MPTP administration (MPTP+Post). Dosage regimens are illustrated in Fig. S4. Statistical analysis was performed using one-way ANOVA and the post-hoc Bonferroni test. Scale bar: 50 μ m. Error bars, mean \pm SEM ns-nonsignificant, ***- $P < 0.001$.

Apart from toxic accumulation of SNCA aggregates as Lewy bodies, proteostasis machineries such as autophagy are also defunct in these dying neurons.⁷ While autophagosome formation has been shown to be defective in PD,⁴ its accumulation has been documented in the striata of human PD postmortem brains.²¹ Also, recent reports suggest that apart from having a misfolding propensity, prion-like properties²² of SNCA are responsible for its spreading across neurons leading to aggravated neuronal death. Hence, enhancing SNCA clearance through modulating autophagy would be beneficial.

We show here using 2 model systems that aggregate clearance by 6-Bio is through autophagy: using yeast genetics, our

studies reveal that 6-Bio is unable to rescue SNCA-mediated cytotoxicity in autophagy-defective mutants, while in mammalian cells, pharmacological inhibition of autophagy by 3-MA abolishes 6-Bio effect. In addition, although 6-Bio (50 μ M) does not affect the growth of yeast cells, it strikingly increases basal autophagy even in growth conditions, a situation where MTOR is active and is known to suppress autophagy. Interestingly, 6-Bio induction of autophagy in mammalian cells appears to be MTOR dependent. Furthermore, 6-Bio not only augments basal autophagy but also enhances the starvation induced autophagy, demonstrating its strong autophagy modulating potential. It is these properties that lead to a dramatic

buildup of autolysosomes upon 6-Bio treatment. Enhanced cargo degradation thus leads to clearing up of the aggregates and preventing cytotoxicity by restoring cellular proteostasis.

The MPTP+6-Bio-treated cohort spent more time on the rotarod (as the placebo cohort) and traveled more distance in open field unlike the MPTP-treated cohort, we therefore can infer that 6-Bio rescued the MPTP-induced motor, locomotion and exploratory impairments. Importantly, 6-Bio-induced behavioral performances were indistinguishable from that of the placebo cohort. Thus, histological and behavioral analyses of the MPTP-induced preclinical mouse model of PD highlights the neuroprotective abilities of 6-Bio as demonstrated by preservation of nigral DAergic neurons and retention of motor coordination functions. After 48 h of MPTP administration, most of the DAergic neurons would be ablated. Thus after 48 h of MPTP treatment, with highly depleted SNpc of DAergic neurons, 6 Bio was unable to rescue behavioral deficits. These results suggest that 6-Bio primarily acts through restoring autophagy function in the neurons to get rid of aggregates and perhaps does not have neuroregenerative capabilities. Strikingly, our experiment revealed that 6-bio enters the brain within 15 min after intraperitoneal administration and stayed as long as 24 h (Table S2). The dramatic neuroprotection could be due to abundance of 6-Bio in the mice brain that facilitates aggregate clearance through inducing autophagy.

Our studies with other GSK3B inhibitors (with similar inhibitory potencies) reveal that none of these can bring about autophagy induction as profoundly as 6-Bio (data not shown). Though 6-Bio has been shown to modulate GSK3, PDK1 and JAK-STAT3 signaling pathways,¹⁸ our results demonstrated that it modulates autophagy in GSK3B dependent manner. 6-Bio docks with GSK3B better than other inhibitors such as indirubin, hymenialdisine and meridianins.²³ It also increases the accumulation of CTNNB1/ β -catenin due to the inhibition GSK3B, thus promoting aggression of breast cancer cells.²⁴ 6-Bio also indirectly activates canonical WNT5A signaling in the hippocampal neurons to protect them from A β oligomers.¹² Proof-of-principle demonstrations at the cellular level reveal that inhibiting GSK3B reduces SNCA expression²⁵ and also results in β -amyloid clearance.²⁶ Thus, GSK3B would be an attractive avenue as a therapeutic target for neurodegeneration. In PD, autophagy is dysfunctional as the steps of autophagosome biogenesis⁴ and the fusion between autophagosome and lysosome are blocked.²⁷ Because 6-Bio dramatically enhances autophagosome-lysosome fusion by inhibiting GSK3B through crossing the blood-brain barrier, it decreases the dramatic toxic protein aggregates in SNpc. Therefore, 6-Bio could be a promising candidate with therapeutic potential especially in case of synucleopathies including PD.

Our findings demonstrate that the neuroprotective role of 6-Bio is due to its autophagosome-lysosome fusion-enhancing function, which results in SNCA aggregate clearance, and thus may have therapeutic potential for patients with PD and protein conformational disorders.

Methods

Chemicals and antibodies

Yeast extract (RM027), peptone (RM667), dextrose (GRM077), galactose (RM101) and amino acids [leucine (GRM054),

methionine (GRM200), histidine (RM051) and uracil (RM264)] were purchased from HiMedia. 3-MA (M9281), 6-Bio (B1686), LOPAC (LO1280), anti-LC3B antibody (L7543), MPTP (methyl-4-phenyl-1,2,3,6-tetrahydropyridine, M0896), DMEM (D5648), DMEM F-12 (D8900), penicillin and streptomycin (P4333), DAB (3,3'-Diaminobenzidine, D3939), Atto 663 (41176), lysine (L5501) and trypsin EDTA (59418C) were purchased from Sigma-Aldrich. Anti-p-RPS6KB1 T389 antibody (9862) and total RPS6KB1 antibody (9202), anti-p-GSK3B S9 antibody (5558) and total GSK3B antibody (9315), anti-p-EIF4EBP1 T37/46 antibody (2855) and total EIF4EBP1 antibody (9452), anti-LAMP1 antibody (9091) and anti-rabbit IgG, horseradish peroxidase (HRP; 7074) antibody were purchased from Cell Signaling Technology. Anti TUBB/ β -Tubulin (MA5-16308) and anti Tdh (MA5-15738) antibodies were purchased from Thermo Scientific. Yeast does not express GAPDH but instead expresses 3 orthologs (Tdh1/2/3) of the mammalian protein, and that the antibody was raised against recombinant GAPDH (Thermo Scientific). While the antibody has been used in yeast studies, publication cannot be interpreted as validation unless there is supporting experimental data that the antibody indeed detects yeast Tdh. Anti-APP/amyloid β oligomer/A11 (AB9234) was purchased from Merck Millipore. Anti-Pgk1 (ab 38007) antibody was purchased from Abcam. Anti-GFP (11 814 460 001) antibody was purchased from Roche. Anti TH/tyrosine hydroxylase (N196) antibody was purchased from Santa Cruz Biotechnology. Anti-mouse IgG, HRP (172-1011) antibody was purchased from Bio-Rad. CMAC-Blue (C2110) was purchased from Life Technologies. Bafilomycin A₁ (11038) was purchased from Cayman chemical. VECTASTAIN Elite ABC Kit (PK-6200) was purchased from VECTOR laboratories.

Plasmid constructs, shRNA and yeast strains

Plasmids used were GFP-Atg8 (pRS316) [gift from Y. Oshumi (Tokyo Institute of Technology)], SNCA-GFP (pRS 306) under the galactose promoter (gift from Paulo Ludovico) and GFP- β A₁₋₄₂ (pRS306). ptfLC3B²⁸ (gift from Tamotsu Yoshimori; Addgene, 21074), GFP-SNCA²⁹ (gift from David Rubinzstein; Addgene, 40822). pLKO.1-GSK3B-#1 was a gift from Alex Toker³⁰ (Addgene, 32496). Scrambled shRNA was a gift from David Sabatini³¹ (Addgene, 1864). All yeast strains in this study are listed in Table S1.

Yeast media, culture conditions, growth assays and SNCA-GFP aggregate induction

Yeast media used for culturing were YPD (yeast extract, peptone and dextrose) for wild-type (WT) GFP and autophagy mutant strains, SD-Ura [synthetic dextrose (2%) medium without uracil] for culturing the SNCA-GFP strain and the GFP-Atg8-processing assay, SG-Ura [synthetic galactose (2%) medium without uracil] to induce SNCA-GFP expression. All strains were cultured at 30°C and 250 rpm.

Growth assays: In a 384-well plate, appropriate yeast strains were seeded ($A_{600} \sim 0.07$) with or without drugs and incubated (80 μ l, 30°C and 420 rpm) in a multiplate reader (Varioskan Flash, Thermo Scientific, USA) for 48 h with automatic

absorbance (A_{600}) recording every 20 min. Growth curves were plotted and analyzed using GraphPad Prism.

Induction of SNCA-GFP aggregates: To induce SNCA-GFP aggregates, the corresponding strains were inoculated in SD-Ura medium. Secondary culture was inoculated from primary inoculum until the absorbance at A_{600} reached 0.8/ml. Cells were washed twice with sterile water and adding SG-Ura for 12 to 16 h induced aggregates.

Small molecule screen

To screen small molecule library LOPAC¹²⁸⁰ in the *S. cerevisiae* SNCA toxicity model, working plates containing 50 μ M drugs in 1.5% DMSO (190 compounds/plate) were prepared in a 384-well format. WT SNCA-GFP with or without small molecules and untreated WT GFP were grown under optimized conditions (80 μ l, 30°C and 420 rpm) for 36 h in a plate reader (Varioskan Flash, Thermo Scientific) in duplicates with automatic absorbance (A_{600}) recording every 20 min. Growth curves of untreated WT GFP and WT SNCA-GFP strains were plotted and mid to late exponential phase time point of untreated WT GFP strain was chosen as reference for data analysis. Its corresponding time point of untreated and drug-treated WT SNCA-GFP strains were plotted separately in a box plot. Small molecules that rescued the growth lag by ≥ 3 SD units of untreated WT SNCA-GFP strain were considered as ‘hits’.

SNCA-GFP degradation assays

To assess SNCA-GFP degradation efficacy by 6-Bio, after inducing SNCA-GFP aggregate, the galactose promoter was turned off by adding dextrose. Cells were treated with 6-Bio (50 μ M) for 0, 6, 12 and 24 h. Subsequent degradation of SNCA-GFP levels were analyzed using immunoblotting (Fig. S4A).

Mammalian cell culture

HeLa cells were maintained in DMEM containing 10% fetal bovine serum (Pan-Biotech, P03–6510). Undifferentiated SH-SY5Y cells were maintained in DMEM-F12 containing 10% fetal bovine serum (Life Technologies, 12500062). Cell lines were cultured in the presence of 5% CO₂ at 37°C. To perform autophagy assays, equal numbers of subconfluent HeLa cells were seeded in 6-well dishes, allowed to attach for 24 h, treated with 6-Bio (5 μ M) and/or 3-MA (5 mM) in growth medium for 2 h. For the GFP-SNCA degradation assay, equal numbers of subconfluent SH-SY5Y cells were seeded in 6-well dishes and allowed to attach for 24 h. Cells were transfected with GFP-SNCA plasmid using Lipofectamine 2000 (Life Technologies, 11668–019) and allowed to express for 24 h. Cells were treated with 6-Bio (5 μ M) for 24 h and fold GFP-SNCA levels were analyzed using immunoblotting.

For the tandem RFP-GFP-LC3B assay, subconfluent cells were seeded in 60-mm dishes, transfected with tandem RFP-GFP-LC3B plasmid construct and allowed to express for 24 h. Later, cells were trypsinized, reseeded (10^5 cells) and allowed to attach on coverslips in a 12-well plate. Cells were treated with or without 6-Bio (5 μ M) for 2 h and coverslips were processed for imaging.

Immunoblot analysis

Preparation of yeast lysates: Yeast strains ($A_{600} = 3$) were resuspended in trichloroacetic acid (12.5%) and stored at -80°C for at least half an hour. Samples were thawed on ice, centrifuged (16000 \times g, 10 min) and the pellet was washed twice with ice-cold acetone (80%). Pellets were air-dried, resuspended in lysis (1% SDS and 0.1 N NaOH) solution and Laemmli buffer and boiled for 10 min.

Preparation of mammalian cell lysates: After treatments, cells were collected in Laemmli buffer to perform the LC3B processing assay, RPS6KB1, GSK3B and EIF4EBP1 immunoblotting. To validate GFP-SNCA degradation by 6-Bio, treated cells were scraped and collected in growth medium. After washing with phosphate buffer, pellets were lysed in Laemmli buffer and boiled for 10 min. Samples were electrophoresed on SDS-PAGE (8–15%) and then transferred onto PVDF (Bio-Rad, 162–0177) membrane using Transblot turbo (Bio-Rad). Transferred blots were stained with Ponceau S, probed with appropriate primary antibodies overnight and subsequently HRP-conjugated secondary antibody. Signals were developed using enhanced chemiluminescence substrate (Clarity, Bio-Rad), imaged using a gel documentation system (G-Box, Syngene, UK) and bands were quantified using ImageJ software (NIH).

GFP-Atg8-processing assay

An *S. cerevisiae* strain with an GFP-Atg8 plasmid was grown in SD-U (synthetic dextrose medium without uracil) under standardized conditions (30°C, 250 rpm). Using this, the secondary culture was inoculated ($A_{600} = 0.2$) and grown under the same standardized conditions until the culture absorbance reached $A_{600} = 0.7$. For assessing the effect of 6-Bio (50 μ M) in inducing autophagy in growth conditions, the cells were transferred to SD-U with 6-Bio for 6 h. To test the effect of 6-Bio in enhancing starvation-induced autophagy, cells were washed twice and transferred to starvation medium with 6-Bio and samples were collected for 0, 2, 4 and 6 h time points.³² Proteins were precipitated using trichloroacetic acid and resolved by SDS-PAGE (10%) followed by immunoblotting. In the blot, “GFP-Atg8 accumulation” indicates the induction of Atg8 expression and “free GFP release” indicates the degradation of GFP-Atg8 in the vacuole. The GFP-Atg8 protein is degraded in the vacuole (yeast lysosome); however, the GFP tag is relatively more resistant to vacuolar hydrolases. The levels of GFP-Atg8 (intact fusion protein) would indicate induction of Atg8 expression (which in turn is interpreted as possible autophagy induction) whereas comparison to the total GFP (summation of GFP signals from both full-length GFP-Atg8 and free GFP) indicates the autophagy flux^{12,33} (turnover of the fusion GFP-Atg8 protein to free GFP).

Microscopy

Yeast cultures after respective treatments were washed, mounted on an agarose (2%) pad and imaged.

For mammalian cell microscopy, after 2 h of treatment, coverslips were fixed using 4% paraformaldehyde (PFA; Sigma, 158127) and permeabilized using Triton X-100 (0.2%;

HiMedia, MB031). Coverslips were mounted using antifade, Vectashield (Vector laboratories, H-1000). For antibody staining, coverslips were blocked in 5% BSA (Sigma, RM105) for 1 h, incubated in primary antibody overnight and subsequently probed with fluorescent-conjugated antibody. Coverslips were mounted using antifade, Vectashield.

Images were acquired using DeltaVision Elite widefield microscope (API, GE, USA) with following filters: DAPI (390/18 and 435/48), FITC (490/20 and 529/38), TRITC (542/27 and 594/45) and Cy5 (632/22 and 676/34). Images were processed using DV SoftWoRX software.

The tandem RFP-GFP-LC3B assay (sometimes referred to as traffic light assay) is one test to assess autophagic flux in mammalian cells.²⁸ In this assay, autophagosomes appear as yellow puncta. Unlike RFP, GFP fluorescence being pH sensitive, gets quenched in the acidic pH environment of autolysosomes and thus appears red.

For the FITC-dextran uptake assay, after drug treatments, the HeLa cells were incubated with FITC-dextran (70 kDa; Sigma, 46945) for 30 min at 2 different temperature conditions (37°C and 16°C).

Cell viability assay

SH-SY5Y cells were seeded on 96-well plates and transfected with a plasmid encoding GFP-SNCA only and/or cotransfected with GSK3B shRNA and GFP-SNCA. To cells, the drugs were added (24 h) after 48 h of transfection. Then, the cell viability was measured using the CellTitre-Glo[®] (Promega, G7570) and luminescence was measured using a Varioskan Flash reader (Thermo Scientific).

Animal studies

All procedures in this study were approved by the JNCASR Institute Animal Ethical Committee (IAEC) and conducted as per the guidelines of the Committee for the Purpose of Control and Supervision of Experiments on Animals (CPCSEA). Inbred male C57BL/6J mice (3 to 4 mo old) were used for all experimental cohorts.

Studies on MPTP mouse PD model

Mice were randomly allocated to 5 different study cohorts, viz., Placebo (n = 5), 6-Bio-only (n = 5), MPTP (n = 5), MPTP+Pro (n = 3) and MPTP+Co (n = 5). As described previously,¹⁹ 23.4 mg/kg MPTP.HCl (equivalent to 20 mg/kg free base) in 10 ml/kg body weight of saline was administered i.p. for 4 times at 2 h intervals. Further, 5 mg/kg body weight of 6-Bio in 100 μ l of saline was administered i.p. to the MPTP-injected animals by following either of the 2 different regimens; the first regimen comprised a prophylactic, pretreatment which was begun 2 d before MPTP administration (MPTP+Pro); while the second involved treatment given alongside the MPTP injection (MPTP+Co). In both the cases, 6-Bio was administered for 7 d post MPTP administration daily (Fig. S5A). The other experimental cohorts included placebo, 6-Bio only (daily i.p.) and MPTP alone (daily vehicle) for 9 d. All mice were

killed 9 d post MPTP administration and brains were processed for immunohistochemistry.

Immunohistochemistry

Mice were anaesthetized using Halothane BP (Piramal Healthcare, India) inhalation and perfused intracardially with normal saline followed by 4% PFA in 0.1 M phosphate buffer, pH 7.4. Mice brains were removed quickly and postfixed with 4% PFA for 24 to 48 h at 4°C. Following cryoprotection in 15 and 30% sucrose (HiMedia, MB025), 40- μ m-thick coronal cryosections of midbrain were collected serially on gelatinized slides. The immunoperoxidase labeling protocol was identical to that reported.³⁴ Briefly, endogenous peroxidase was quenched using H₂O₂ (0.1%) in methanol (70%), followed by blocking of non-specific staining by a buffered solution (3%) of BSA for 4 h at room temperature. Sections were incubated with TH primary antibody (1:500) followed by biotin-conjugated secondary antibody (1:200 dilution; Vector Laboratories, BA-1400). Tertiary labeling was performed with avidin-biotin complex solution (1:100; Vector Laboratories, PK-6200). Staining was visualized using 3'-3'-diaminobenzidine (0.05%; Sigma, D3939) as a chromogen in a solution of 0.1 M acetate imidazole buffer (pH 7.4) and H₂O₂ (0.1%). Negative controls were processed identically, except that the primary antibody was replaced with dilution buffer.

For immunofluorescent-based double labeling, the sequential staining procedure was followed.³⁵ Brain sections were stained for TH and LC3B-APP/amyloid β oligomer/A11 and images were acquired using a DeltaVision Elite widefield microscope (API, GE).

Stereological quantification of TH⁺ DAergic neurons in SNpc

As described,³⁶ SNpc was delineated using the 4X objective of Olympus BX61 Microscope (Olympus, Japan) equipped with Stereo Investigator Software Version 7.2 (Micro Bright Field, USA). Stereological quantification was performed using optical fractionator probe with slight modifications.³⁶ Briefly, every sixth midbrain section containing SNpc was chosen and TH⁺ cells were counted under the 100X objective, with a regular grid interval of 22,500 μ m² (x = 150 μ m, y = 150 μ m) and counting frame with an area of 3600 μ m² (x = 60 μ m, y = 60 μ m). Mounted thickness was determined at every fifth site, which averaged to 25 μ m. A guard zone of 4 μ m was applied on either side, thus providing 17 μ m of z-dimension within the optical disector. The quantification was performed starting with the first anterior appearance of TH⁺ neurons in SNpc to the caudal-most part. The SNpc volume was determined by planimetry and total numbers of neurons according to mean measured thickness were noted.

Densitometry-based image analysis

We used high magnification images of TH-stained nigral DAergic neurons, captured for offline assessment of expression levels. Expression intensity was measured using a Windows-based image analysis system (Q Win V3, Leica Systems,

Germany). Cumulative mean was derived from the values obtained from sampling, approximately 200 DAergic neurons per animal. Intensity output measured on a grayscale of 0 to 255, where 0 equals intense staining and 255 means absence of staining. Thus, lower gray values suggest higher protein expression and vice versa.

In vivo blood brain barrier assay

Animals were randomly allocated for placebo control and drug treatment cohorts. C57BL/6J mice were injected with placebo control or 6-Bio (5 mg/kg of body weight, intraperitoneally) twice with a 24 h time interval. After second injection, the brains were harvested at 15 min, 30 min, 60 min, 6 h, 12 h and 24 h by cervical dislocation. Mice brains were immediately homogenized with RIPA buffer [25 mM Tris-HCL, 150 mM sodium chloride, 1% NP-40 (Roche, 11332473001), 1% sodium deoxycholate (Sigma-Aldrich, D6750) and 0.1% sodium dodecyl sulfate with protease inhibitor cocktail (Roche, 11836170001)] for both treatment cohorts. Homogenously macerated mouse brain sample (100 μ l) was mixed with acetonitrile (ACN, 400 μ l), formic acid (0.2%) and aceclofenac (100 ng/ml, an internal standard; Sigma, A8861), vortexed for 10 min at 2000 rpm Orbital shaker (compact digital microplate shaker, 88880024, Thermo Scientific, USA). Then, samples were centrifuged and the supernatant was injected for LC MS/MS. Standard samples were prepared by spiking 6-Bio standard into a blank control brain sample. Standard spiking was performed such that resultant concentrations were 0, 10, 100, 500, 1000, 1500 and 2000 ng/ml of drug in blank brain matrix. For LC, PE 200 (Perkin Elmer, USA) HPLC with an Agilent Zorbax XDB C8 4.6 \times 75 mm, 3.5- μ m column (Agilent Technologies, USA) was used. The following conditions were used for LC: Mobile phases (0.1% formic acid in water (5%):methanol (95%)), isocratic flow rate (0.7 ml/min), run time (4 min), injection volume (15 μ l) and needle wash solution (1:1 methanol:water mix containing 0.1% formic acid). The mass spectrometry (API3000, AB Sciex, USA) was used with aceclofenac as an internal control and data were processed using Analyst Software V1.4.2. Drug injections of the various cohorts and preparations of the brain homogenates were performed at JNCASR. Acquity laboratories, India performed the above mentioned LC-MS/MS analysis of the brain samples.

Behavioral studies

Behavioral procedures used for this study were modified from.³⁷⁻⁴⁰ All the behavioral experiments were done on 3- to 4-mo-old male C57BL/6J mice. Experimenters were blind to the drug injected animals. Experimenters handled mice used for behavioral experiments for 3 consecutive d before the training paradigm. Behavioral experiments were designed in an order of low- to high-stress activity for mice. Therefore, the open field test was conducted in the forenoon whereas the rotarod was performed in the afternoon. Mice were habituated to the behavior room for 15 min every day before the start of experiments. The light

intensity was maintained at 100 lx throughout the experiment. Mice were weighed every day before training or test to ensure their good health. Mice were randomly allocated into 3 treatment cohorts: placebo control, MPTP and 6-Bio. Data were plotted using GraphPad prism 5 software.

Rotarod trials

The rotarod instrument was custom made at the mechanical workshop, National Center for Biological Sciences, Bengaluru, India. The rotating rod (diameter 3.3 cm) was made of Delrin and was textured to enhance the grip of mice. The rod was fixed at a height of 30 cm from the cushioned platform where mice fell on to during training and test. The rod was partitioned into 3 areas of 9.3-cm distance between each partition using discs (40-cm diameter) made of Teflon. Mice were trained in the rotarod for 5 consecutive d before drug injection. Each mouse was trained in the rotarod by gradually increasing the rotation on every day. On d 1, mice were trained on 5 to 10 rpm (accelerated at 1 rpm/5 seconds), 11 to 15 rpm (accelerated at 1 rpm/5 seconds) on second day, 16 to 20 rpm (accelerated at 1 rpm/5 seconds) on the third d and at 20 rpm (fixed) for d 4 and 5. Mice were trained at the above specific rpm for 3 times with 5-min interval between trials. The rod was rotated from 5 rpm to 20 rpm by manually changing the speed of the motor (nonautomated). During the test (d 13 postinjection), the rotarod was started at 20 rpm. Mice were tested in a rotating rotarod for a maximum of 60 seconds and their latencies were noted down. At the end of each trial, the rotarod was wiped with 70% ethanol and left for drying before placing the next set of mice. The entire trial was video recorded using a DSLR camera (Nikon D5100, India) and latencies were scored manually. The average time spent on the rotating rotarod across 3 trials were plotted as mean latency to fall.

Open field test

The open field arena (50 cm \times 50 cm \times 45 cm) was custom-made (JNCASR) using plywood and the internal surface was coated with white polish. Mice were trained in the open field for 2 consecutive days before drug injection. During training or testing, one animal at a time was placed in the zone periphery in the open field arena and allowed to explore the arena for 5 min. The activity was video recorded (SONY[®] color video camera, Model no. SSC-G118, India) using software (SMART v3.0.04 from Panlab, Harvard Apparatus, USA). After 5 min, the mouse was returned to its home cage. The open field arena was then wiped using 70% ethanol and allowed to dry before placing the next mouse. Distances traveled were analyzed offline by an experimenter who was not involved in performing the experiment.

Statistical analysis

Statistical analyses were performed using the unpaired Student *t* test and ANOVA (one-way or 2-way) followed by the post-hoc Bonferroni test in GraphPad Prism. Error bars were expressed as mean \pm SEM.

Abbreviations

A ₆₀₀ ,	absorbance at 600 nm;
6-Bio,	6-Bromindirubin-3'-oxime;
DA,	dopamine;
GFP,	green fluorescent protein;
GSK3B,	glycogen synthase kinase 3.
HRP,	horseradish peroxidase;
i.p.,	intraperitoneally;
LOPAC,	Library of Pharmacologically Active Compounds;
3-MA,	3-methyladenine;
MAP1LC3B/LC3B,	microtubule associated protein 1 light chain 3 β ;
MPTP,	1-methyl-4-phenyl-1,2,3,6-tetrahydropyridine;
PD,	Parkinson disease;
Pep A,	pepstatin A;
Pgk1,	phosphoglycerate kinase 1;
RFP,	red fluorescent protein;
SD,	standard deviation;
SEM,	standard error mean;
SNpc,	substantia nigra pars compacta;
TH,	tyrosine hydroxylase;

Disclosure of potential conflicts of interest

No potential conflicts of interest were disclosed.

Acknowledgments

We thank Y. Ohsumi, Paulo Ludovico, Tamotsu Yoshimori and David Rubinzstein for the kind gift of plasmids and Prof. MRS Rao, Dr. Subba Rao, Dr. K. Vijayachandra, Dr. Prathibha Ranganathan, Dr. Tej Kumar Pareek, Aparna Hebbar and members of the autophagy laboratory (JNCASR) for critical reading of the manuscript. Dr. Prakash and Muthumenakshi Bhaskaran's help in animal facility at JNCASR is acknowledged. We thank Dr. Alicia Brantley, Director, Behavior Core and Dr. Thomas Creson, Staff Scientist, Scripps Research Institute, Florida for their valuable suggestions on behavioral experiments.

Funding

This work was supported by the Wellcome Trust/DBT India Alliance Intermediate Fellowship awarded to RM (500159-Z-09-Z), JNCASR intramural funds to RM, DST-SERB (SR/SO/HS/0121/2012) to PAA and DST-SERB (SB/YS/LS-215/2013) to JPC. Application of 6-Bio in autophagy modulation and neurodegeneration is patent pending.

References

- [1] Mortality GBD, Causes of Death C. Global, regional, and national age-sex specific all-cause and cause-specific mortality for 240 causes of death, 1990-2013: a systematic analysis for the Global Burden of Disease Study 2013. *Lancet* 2015; 385:117-71; PMID:25530442; [https://doi.org/10.1016/S0140-6736\(14\)61682-2](https://doi.org/10.1016/S0140-6736(14)61682-2)
- [2] German DC, Manaye K, Smith WK, Woodward DJ, Saper CB. Midbrain dopaminergic cell loss in Parkinson's disease: computer visualization. *Ann Neurol* 1989; 26:507-14; PMID:2817827; <https://doi.org/10.1002/ana.410260403>
- [3] Thanvi B, Lo N, Robinson T. Levodopa-induced dyskinesia in Parkinson's disease: clinical features, pathogenesis, prevention and treatment. *Postgraduate Med J* 2007; 83:384-8; PMID:17551069; <https://doi.org/10.1136/pgmj.2006.054759>
- [4] Nixon RA. The role of autophagy in neurodegenerative disease. *Nat Med* 2013; 19:983-97
- [5] Hara T, Nakamura K, Matsui M, Yamamoto A, Nakahara Y, Suzuki-Migishima R, Yokoyama M, Mishima K, Saito I, Okano H, et al. Suppression of basal autophagy in neural cells causes neurodegenerative disease in mice. *Nature* 2006; 441:885-9; PMID:16625204; <https://doi.org/10.1038/nature04724>
- [6] Komatsu M, Waguri S, Chiba T, Murata S, Iwata J, Tanida I, Ueno T, Koike M, Uchiyama Y, Kominami E, et al. Loss of autophagy in the central nervous system causes neurodegeneration in mice. *Nature* 2006; 441:880-4; PMID:16625205; <https://doi.org/10.1038/nature04723>
- [7] Liang CC, Wang C, Peng X, Gan B, Guan JL. Neural-specific deletion of FIP200 leads to cerebellar degeneration caused by increased neuronal death and axon degeneration. *J Biol Chem* 2010; 285:3499-509; PMID:19940130; <https://doi.org/10.1074/jbc.M109.072389>
- [8] Sarkar S, Perlstein EO, Imarisio S, Pineau S, Cordenier A, Maglathlin RL, Webster JA, Lewis TA, O'Kane CJ, Schreiber SL, et al. Small molecules enhance autophagy and reduce toxicity in Huntington's disease models. *Nat Chem Biol* 2007; 3:331-8; PMID:17486044; <https://doi.org/10.1038/nchembio883>
- [9] Anguiano J, Garner TP, Mahalingam M, Das BC, Gavathiotis E, Cuervo AM. Chemical modulation of chaperone-mediated autophagy by retinoic acid derivatives. *Nat Chem Biol* 2013; 9:374-82; PMID:23584676; <https://doi.org/10.1038/nchembio.1230>
- [10] Rajasekhar K, Suresh SN, Manjithaya R, Govindaraju T. Rationally designed peptidomimetic modulators of abeta toxicity in Alzheimer's disease. *Scientific Reports* 2015; 5:8139; PMID:25633824; <https://doi.org/10.1038/srep08139>
- [11] Llorens-Martin M, Jurado J, Hernandez F, Avila J. GSK-3beta, a pivotal kinase in Alzheimer disease. *Front Mol Neurosci* 2014; 7:46; PMID:24904272; <https://doi.org/10.3389/fnmol.2014.00046>
- [12] Silva-Alvarez C, Arrazola MS, Godoy JA, Ordenes D, Inestrosa NC. Canonical Wnt signaling protects hippocampal neurons from Abeta oligomers: role of non-canonical Wnt-5a/Ca(2+) in mitochondrial dynamics. *Frontiers Cell Neurosci* 2013; 7:97; PMID:23805073; <https://doi.org/10.3389/fncel.2013.00097>
- [13] Outeiro TF, Lindquist S. Yeast cells provide insight into alpha-synuclein biology and pathobiology. *Science* 2003; 302:1772-5; PMID:14657500; <https://doi.org/10.1126/science.1090439>
- [14] Khurana V, Lindquist S. Modelling neurodegeneration in *Saccharomyces cerevisiae*: why cook with baker's yeast? *Nat Rev Neurosci* 2010; 11:436-49; PMID:20424620; <https://doi.org/10.1038/nrn2809>
- [15] Outeiro TF, Kontopoulos E, Altmann SM, Kufareva I, Strathearn KE, Amore AM, Volk CB, Maxwell MM, Rochet JC, McLean PJ, et al. Sirtuin 2 inhibitors rescue alpha-synuclein-mediated toxicity in models of Parkinson's disease. *Science* 2007; 317:516-9; PMID:17588900; <https://doi.org/10.1126/science.1143780>
- [16] Polychronopoulos P, Magiatis P, Skaltsounis AL, Myrianthopoulos V, Mikros E, Tarricone A, Musacchio A, Roe SM, Pearl L, Leost M, et al. Structural basis for the synthesis of indirubins as potent and selective inhibitors of glycogen synthase kinase-3 and cyclin-dependent kinases. *J Med Chem* 2004; 47:935-46; PMID:14761195; <https://doi.org/10.1021/jm031016d>
- [17] Grassilli E, Ianzano L, Bonomo S, Missaglia C, Cerrito MG, Giovannoni R, Masiero L, Lavitrano M. GSK3A is redundant with GSK3B in modulating drug resistance and chemotherapy-induced necroptosis. *PLoS One* 2014; 9:e100947; PMID:24984063; <https://doi.org/10.1371/journal.pone.0100947>
- [18] Braig S, Kressirer CA, Liebl J, Bischoff F, Zahler S, Meijer L, Vollmar AM. Indirubin derivative 6BIO suppresses metastasis. *Cancer Res* 2013; 73:6004-12; PMID:23946383; <https://doi.org/10.1158/0008-5472.CAN-12-4358>
- [19] Jackson-Lewis V, Przedborski S. Protocol for the MPTP mouse model of Parkinson's disease. *Nat Protocols* 2007; 2:141-51; PMID:17401348; <https://doi.org/10.1038/nprot.2006.342>
- [20] Li XZ, Chen XP, Zhao K, Bai LM, Zhang H, Zhou XP. Therapeutic effects of valproate combined with lithium carbonate on MPTP-induced parkinsonism in mice: possible mediation through enhanced autophagy. *Int J Neurosci* 2013; 123:73-9; PMID:22978383; <https://doi.org/10.3109/00207454.2012.729234>

- [21] Anglade P, Vyas S, Hirsch EC, Agid Y. Apoptosis in dopaminergic neurons of the human substantia nigra during normal aging. *Histol Histopathol* 1997; 12:603-10; PMID:9225140
- [22] Luk KC, Kehm V, Carroll J, Zhang B, O'Brien P, Trojanowski JQ, Lee VM. Pathological alpha-synuclein transmission initiates Parkinson-like neurodegeneration in nontransgenic mice. *Science* 2012; 338:949-53; PMID:23161999; <https://doi.org/10.1126/science.1227157>
- [23] Nisha CM, Kumar A, Vimal A, Bai BM, Pal D, Kumar A. Docking and ADMET prediction of few GSK-3 inhibitors divulges 6-bromoindirubin-3-oxime as a potential inhibitor. *J Mol Graphics Modelling* 2016; 65:100-7; PMID:26967552; <https://doi.org/10.1016/j.jmngm.2016.03.001>
- [24] Yasuhara R, Irie T, Suzuki K, Sawada T, Miwa N, Sasaki A, Tsunoda Y, Nakamura S, Mishima K. The beta-catenin signaling pathway induces aggressive potential in breast cancer by up-regulating the chemokine CCL5. *Exp Cell Res* 2015; 338:22-31; PMID:26363360; <https://doi.org/10.1016/j.yexcr.2015.09.003>
- [25] Golpich M, Amini E, Hemmati F, Ibrahim NM, Rahmani B, Mohamed Z, Raymond AA, Dargahi L, Ghasemi R, Ahmadiani A. Glycogen synthase kinase-3 beta (GSK-3beta) signaling: Implications for Parkinson's disease. *Pharmacological Res* 2015; 97:16-26; PMID:25829335; <https://doi.org/10.1016/j.phrs.2015.03.010>
- [26] Parr C, Carzaniga R, Gentleman SM, Van Leuven F, Walter J, Sastre M. Glycogen synthase kinase 3 inhibition promotes lysosomal biogenesis and autophagic degradation of the amyloid-beta precursor protein. *Mol Cell Biol* 2012; 32:4410-8; PMID:22927642; <https://doi.org/10.1128/MCB.00930-12>
- [27] Ejlertskov P, Hultberg JG, Wang J, Carlsson R, Ambjorn M, Kuss M, Liu Y, Porcu G, Kolkova K, Friis Rundsten C, et al. Lack of Neuronal IFN-beta-IFNAR Causes Lewy Body- and Parkinson's Disease-like Dementia. *Cell* 2015; 163:324-39; PMID:26451483; <https://doi.org/10.1016/j.cell.2015.08.069>
- [28] Kimura S, Noda T, Yoshimori T. Dissection of the autophagosome maturation process by a novel reporter protein, tandem fluorescently-tagged LC3. *Autophagy* 2007; 3:452-60; PMID:17534139
- [29] Furlong RA, Narain Y, Rankin J, Wyttenbach A, Rubinsztein DC. Alpha-synuclein overexpression promotes aggregation of mutant huntingtin. *Biochem J* 2000; 346 Pt 3:577-81; PMID:10698681
- [30] Yoeli-Lerner M, Chin YR, Hansen CK, Toker A. Akt/protein kinase b and glycogen synthase kinase-3beta signaling pathway regulates cell migration through the NFAT1 transcription factor. *Mol Cancer Res* 2009; 7:425-32; PMID:19258413; <https://doi.org/10.1158/1541-7786.MCR-08-0342>
- [31] Sarbassov DD, Guertin DA, Ali SM, Sabatini DM. Phosphorylation and regulation of Akt/PKB by the rictor-mTOR complex. *Science* 2005; 307:1098-101; PMID:15718470; <https://doi.org/10.1126/science.1106148>
- [32] Rajasekhar K, Narayanaswamy N, Mishra P, Suresh SN, Manjithaya R, Govindaraju T. Synthesis of Hybrid Cyclic Peptoids and identification of autophagy enhancer. *Chempluschem* 2014; 79:25-30
- [33] Graef M, Nunnari J. Mitochondria regulate autophagy by conserved signalling pathways. *EMBO J* 2011; 30:2101-14; PMID:21468027; <https://doi.org/10.1038/emboj.2011.104>
- [34] Alladi PA, Mahadevan A, Yasha TC, Raju TR, Shankar SK, Muthane U. Absence of age-related changes in nigral dopaminergic neurons of Asian Indians: relevance to lower incidence of Parkinson's disease. *Neuroscience* 2009; 159:236-45; PMID:19135503; <https://doi.org/10.1016/j.neuroscience.2008.11.051>
- [35] Vidyadhara DJ, Yarreiphang H, Raju TR, Alladi PA. Admixing of MPTP-resistant and susceptible mice strains augments Nigrostriatal Neuronal Correlates to Resist MPTP-Induced Neurodegeneration. *Mol Neurobiol* 2016; PMID:27704331; <https://doi.org/10.1007/s12035-016-0158-y>
- [36] Fu Y, Yuan Y, Halliday G, Rusznak Z, Watson C, Paxinos G. A cytoarchitectonic and chemoarchitectonic analysis of the dopamine cell groups in the substantia nigra, ventral tegmental area, and retrorubral field in the mouse. *Brain Struct Funct* 2012; 217:591-612; PMID:21935672; <https://doi.org/10.1007/s00429-011-0349-2>
- [37] Liu W, Jalewa J, Sharma M, Li G, Li L, Holscher C. Neuroprotective effects of lixisenatide and liraglutide in the 1-methyl-4-phenyl-1,2,3,6-tetrahydropyridine mouse model of Parkinson's disease. *Neuroscience* 2015; 303:42-50; PMID:26141845; <https://doi.org/10.1016/j.neuroscience.2015.06.054>
- [38] Patil SP, Jain PD, Ghumatkar PJ, Tambe R, Sathaye S. Neuroprotective effect of metformin in MPTP-induced Parkinson's disease in mice. *Neuroscience* 2014; 277:747-54; PMID:25108167; <https://doi.org/10.1016/j.neuroscience.2014.07.046>
- [39] Brooks SP, Dunnett SB. Tests to assess motor phenotype in mice: a user's guide. *Nat Rev Neurosci* 2009; 10:519-29; PMID:19513088; <https://doi.org/10.1038/nrn2652>
- [40] Buccafusco JJ. The revival of scopolamine reversal for the assessment of cognition-enhancing drugs. In: Buccafusco JJ, ed. *Methods of behavior analysis in neuroscience*. Boca Raton (FL): CRC Press; 2009.